Journal of Coordination Chemistry
Publication details, including instructions for authors and subscription information:
http://www.tandfonline.com/loi/gcoo20

Designing a new organic-inorganic arsenomolybdate by modification of traditional Keggin-type building fragment

Xiang Ma [a], Suzhi Li [a b], Jiai Hua [a], Pengtao Ma [a], Jingping Wang [a] & Jingyang Niu [a]

[a] Institute of Molecular and Crystal Engineering, College of Chemistry and Chemical Engineering, Henan University, Kaifeng, 475004, P. R. China

[b] College of Chemistry and Chemical Engineering, Shangqiu Normal University, Shangqiu Henan, 476000, P. R. China

Accepted author version posted online: 29 Jan 2013.Published online: 05 Mar 2013.

To cite this article: Xiang Ma, Suzhi Li, Jiai Hua, Pengtao Ma, Jingping Wang & Jingyang Niu (2013) Designing a new organic-inorganic arsenomolybdate by modification of traditional Keggin-type building fragment, Journal of Coordination Chemistry, 66:4, 725-736, DOI: 10.1080/00958972.2013.770484

To link to this article: http://dx.doi.org/10.1080/00958972.2013.770484

Journal of Coordination Chemistry
Vol. 66, No. 4, 20 February 2013, 725–736

Designing a new organic–inorganic arsenomolybdate by modification of traditional Keggin-type building fragment

XIANG MA†, SUZHI LI†‡, JIAI HUA†, PENGTAO MA†, JINGPING WANG*† and JINGYANG NIU*†

†Institute of Molecular and Crystal Engineering, College of Chemistry and Chemical Engineering, Henan University, Kaifeng, P.R. China
‡College of Chemistry and Chemical Engineering, Shangqiu Normal University, Shangqiu Henan, P.R. China

(*Received 6 April 2012; in final form 28 November 2012*)

A rare monocapped trivacant Keggin fragment $[A\text{-}\alpha\text{-}As^{III}As^{V}Mo_9O_{34}]^{6-}$ has been captured and an organic–inorganic hybrid arsenomolybdate (AM) $(H_2en)[Ni(en)_2(H_2O)]\{[Ni(en)_2][As^{III}As^{V}Mo_9O_{34}]\}\cdot 3H_2O$ (1) was obtained under hydrothermal conditions. The structure of 1 was determined by X-ray single-crystal diffraction and further characterized by IR spectroscopy, X-ray powder diffraction, scanning electron microscope with energy dispersive X-ray, and X-ray photoelectron spectroscopy. Single-crystal structural analysis indicates that 1 contains the peculiar monocapped trivacant $[A\text{-}\alpha\text{-}As^{III}As^{V}Mo_9O_{34}]^{6-}$ fragment derived from the rare trivacant Keggin-type $[A\text{-}\alpha\text{-}As^{V}Mo_9O_{34}]^{9-}$ unit capped by a triangular pyramidal $\{AsO_3\}$ group. Compound **1** represents the first Ni-substituted inorganic–organic AM containing the $[A\text{-}\alpha\text{-}As^{III}As^{V}Mo_9O_{34}]^{6-}$ subunit.

Keywords: Polyoxometalate; Arsenomolybdate; Monocapped trivacant; Hydrothermal condition

1. Introduction

Polyoxometalates (POMs), as a class of metal-oxygen clusters [1,2], receive attention for compositional diversity, structural versatility and potential applications in catalysis, analytic chemistry, medicine and materials science [3–7]. An important part in this field is transition-metal (TM)-substituted POMs (TMSPs), and a variety of TM-substituted heteropolytungstates with fascinating structures and properties have been obtained [8–13]. In comparison, investigations on TM-substituted heteropolymolybdates (HPMs) are scarce and focused on phosphomolybdates, silicomolybdates, and germanomolybdates [14–18]. Only a few arsenomolybdates (AMs) have been synthesized, $[Mn_2(As^{V}Mo_9O_{33})_2]^{10-}$ [19], $[H_4As^{III}{}_2As^{V}Mo^{V}{}_8Mo^{VI}{}_4O_{40}]^{-}$ [20], $[(Co^{II}O_6)Mo^{VI}{}_6O_{18}(As^{III}{}_3O_3)_2]^{4-}$ [21], $[Himi]_6[As_2Mo_{18}O_{62}]\cdot 11H_2O$ [22], and $[\{Cu(imi)_2\}_3As_3Mo_3O_{15}]\cdot H_2O$ [23]. In contrast with AMs based on traditional fragments, the unconventional POM building blocks utilized in AMs are infrequent owing to the lacunary heteropolyarsenomolybdate behaviors with structural liability in aqueous solution. In 2007, Wang *et al.* reported a series of inorganic–organic

*Corresponding author. Email: jpwang@henu.edu.cn (J.-P. Wang); jyniu@henu.edu.cn (J.-Y. Niu).

Journal of Coordination Chemistry
ISSN 0095-8972 print/ISSN 1029-0389 online
http://dx.doi.org/10.1080/00958972.2013.770484

hybrid AMs constructed from dicapped Anderson-type $[(ZnO_6)(As_3O_3)Mo_6O_{18}]^{4-}$ and $[H_xAs_2Mo_6O_{26}]^{(6-x)-}$ units [24], which broaden our vision and provide us direction in designing and synthesizing HPMs. Recently, Xue *et al.* addressed a series of iso-/hetero-TM sandwich-type AM polyoxoanions such as $[M_2(AsMo_7O_{27})_2]^{n-}$ ($M = Cr^{III}$, $n = 12$; $M = Cu^{II}$, $n = 14$) and $[CrFe(AsMo_7O_{27})_2]^{12-}$ based on the pentavacant $[As^{III}Mo_7O_{27}]^{9-}$ fragments [25] and a cagelike AM fragment $[AgAs_2Mo_{15}O_{54}]^{11-}$ [26], which indicate potential in exploring HPMs. Reports on TM-substituted AMs containing untraditional fragments are rare; most are purely inorganic and synthesized with conventional aqueous solutions, which provide us opportunity to synthesize inorganic–organic hybrid AMs based on unconventional building blocks under hydrothermal conditions.

We are dedicated to investigating the {As-O-Mo} system and very recently prepared a series of inorganic–organic hybrid AMs, $[Cu(en)_2H_2O]_2\{[Cu(en)_2][Cu(en)_2As^{III}As^{V}Mo_9O_{34}]\}_2\cdot 3H_2O$, $(H_2en)_{1.5}[Cu(en)(Hen)][As^{III}As^{V}Mo_9O_{34}]_3\cdot 2H_2O$, and $[Cu(dap)_2]_4[Cu(dap)_2(H_2O)][Cu(dap)_2(As^{III}As^{V}Mo_9O_{34})_2]\cdot 2H_2O$, derived from monocapped trivacant $[A\text{-}\alpha\text{-}As^{III}As^{V}Mo_9O_{34}]^{6-}$ fragments [27]. That As^{III} is partially oxidized to As^{V} may be related to system temperature. In continuation, we work out the influence of controlling temperature on oxidation of As^{III}. We synthesized an organic–inorganic TM-substituted AM built from monocapped trivacant fragment $[A\text{-}\alpha\text{-}As^{III}As^{V}Mo_9O_{34}]^{6-}$, $[H_2en][Ni(en)_2][Ni(en)_2(H_2O)][As^{III}As^{V}Mo_9O_{34}]\cdot 3H_2O$ (**1**), which demonstrates that changing temperature can control the oxidation of As^{III} and that As^{III} and As^{V} can coexist in the synthesis temperature range of 130–150 °C. To the best of our knowledge, **1** represents the first Ni-substituted inorganic–organic hybrid AM constructed from $[A\text{-}\alpha\text{-}As^{III}As^{V}Mo_9O_{34}]^{6-}$.

2. Experimental

All chemicals used for the synthesis were reagent grade and used without purification.

2.1. *Preparation of 1*

Compound **1** was prepared from hydrothermal reaction. Two solutions were prepared separately: solution A: $Na_2MoO_4\cdot 2H_2O$ (0.505 g, 2.085 mmol) and $NaAsO_2$ (0.270 g, 2.078 mmol) were dissolved in 8 mL H_2O under stirring; solution B: $NiCl_2\cdot 2H_2O$ (0.375 g, 1.578 mmol), 1,10-phenanthroline (0.025 g, 0.126 mmol) and en (0.025 mL, 0.374 mmol) were added to 5 mL H_2O under stirring. Then, solution B was added to solution A. The pH of the mixture was adjusted to 6.0 with 4 M HCl, and the mixture was kept at 85 °C on an oil bath for 1.0 h. Finally, the mixture was sealed in a 20 mL Teflon-lined stainless steel autoclave and heated at 130 °C for 3 days under autogenous pressure. After slowly cooling to ambient temperature for 48 h, dark red block crystals were isolated, washed with distilled water, and dried at ambient temperature (28% yield based on $Na_2MoO_4\cdot 2H_2O$).

2.2. *Physical measurements*

IR spectra were obtained from a sample powder palletized with KBr on a Nicolet 170 SXFT-IR spectrophotometer from 4000 to 400 cm^{-1}. X-ray powder diffraction (XRPD) measurements were obtained using a Philips X'pert-MPD instrument with Cu-Kα radiation ($\lambda = 1.54056$ Å) at 293 K. Scanning electron microscope with energy dispersive X-ray

Table 1. Crystallographic data and structural refinements for **1**.

Empirical	$C_{10}H_{48}As_2Mo_9N_{10}Ni_2O_{38}$
Formula weight	2047.30
T (K)	296(2)
Crystal system	Orthorhombic
Space group	$P2(1)2(1)2(1)$
a (Å)	12.911(3)
b (Å)	13.577(3)
c (Å)	27.602(6)
V (Å^3)	4839(2)
Z	4
D_c (g cm^{-3})	2.810
μ (mm^{-1})	4.477 mm^{-1}
$F(000)$	3928
Crystal size (mm^3)	$0.21 \times 0.14 \times 0.07$
θ range for data collections	2.10–25.00°
Limiting indices	$-15 \leqslant h \leqslant 15$ $-15 \leqslant k \leqslant 16$ $-32 \leqslant l \leqslant 24$
Reflections collected	24,902
Independent reflections	8507($R_{int} = 0.0526$)
Refinement method	Full-matrix least-squares on F^2
Goodness-of-fit on F^2	1.014
R_1, wR_2 [$I > 2\sigma(I)$]	0.0408, 0.0810
R_1, wR_2 [all data]	0.0509, 0.0846

(EDX-SEM) analyzes were taken by using a D8 Advance X-ray diffraction analyzer Bruker AXS Microanalysis GmbH. X-ray photoelectron spectroscopy (XPS) were recorded on an Axis Ultra (Kratos, UK) photoelectron spectroscope using monochromatic Al Kα (1486.7 eV) radiation.

2.3. *X-ray crystallography*

Intensity data of **1** were collected on a Bruker Apex-2 CCD detector using graphite monochromated Mo K radiation ($\lambda = 0.71073$ Å) at 296 K. Data integration was performed using *SAINT* [28]. Routine Lorentz and polarization corrections were applied. Multiscan absorption corrections were performed using *SADABS* [29]. The structure was solved by direct methods and refined using full-matrix least squares on F^2. The remaining atoms were found from successive full-matrix least-squares refinements on F^2 and Fourier syntheses. All calculations were performed using the SHELXL-97 program package [30]. No hydrogens associated with water were located from the difference Fourier map. Hydrogens attached to carbon and nitrogen were geometrically placed. All hydrogens were refined isotropically as a riding mode using the default SHELXTL parameters. A summary of crystal data and structure refinements for **1** is listed in table 1.

3. Results and discussion

3.1. *Synthesis*

Parallel experiments show that reaction temperature, organic ligands, and pH play important roles in the formation and crystallization of **1**, especially, the reaction temperature.

Table 2. The summary of synthetic information about some representative AM fragments originated from As^{III} relevant to temperature.

Formula	T (°C)	Synthetic method	Molar ratio of some essential materials	pH
$[MM'(AsMo_7O_{27})_2]^{n-}$ (MM′ = FeFe, CrFe and CrCr) [25]	80	Solvent evaporation	$As_2O_3 : (NH_4)_6Mo_7O_{24}\cdot 2H_2O$: TM =1 : 2 : 2	6.5
$[AgAs_2Mo_{15}O_{54}]^{11-}$ [26]	90	Solvent evaporation	$As_2O_3 : (NH_4)_6Mo_7O_{24}\cdot 2H_2O$: $AgNO_3$ = 1 : 2 : 1	7.0
$(H_2en)_3[(NiO_6)Mo_6O_{18}\ (As_3O_3)_2]Cl_2\cdot 6H_2O$ [33]	90	Solvent evaporation	$NaAsO_2 : Na_2MoO_4\cdot 2H_2O$: ethylenediamine = 1.7 : 1.7 : 45	6.1
$(As_6CuMo_6O_{30})\{[Cu(imi)_4]_3[As_6CuMo_6O_{30}]\}_2\cdot 6H_2O$ [34]	90	Solvent evaporation	$As_2O_3 : (NH_4)_6Mo_7O_{24}\cdot 2H_2O$: imidazole/1,2-propane diamine/ Acetic acid= 2.4 : 0.7 : 4.8	6.0
$[Cu(enMe)_2]_3[As_3Mo_3O_{15}]_3\cdot 2\ H_2O$				
$(NH_4)_{10}\{Cu(H_2O)_4\}[AsMo_6O_{21}(OAc)_3]_2\cdot 12H_2O$				
$[As^{III}_2Fe^{III}_5MMo_{22}O_{85}(H_2O)]^{n-}$ (M = Fe^{3+}, n = 14; M = Ni^{2+} and Mn^{2+}, n = 15) [35]	90	Solvent evaporation	As_2O_3 : $(NH_4)_6Mo_7O_{24}\cdot 2H_2O$ = 1 : 2	6.0
$[Cu(en)_2H_2O]_2\{[Cu(en)_2][Cu(en)_2As^{III}As^{V}Mo_9O_{34}]\cdot 4H_2O$ [27]	130	Hydrothermal conditions	$As_2O_3 : Na_2MoO_4\cdot 2H_2O$: TM : ethylenediamine/1,2-diaminopropane = 0.6 : 2.0 : 1.5/ 1.2 : 1.2	5.4 4.6 6.4
$(H_2en)_{1.5}[Cu(en)(Hen)][As^{III}As^{V}Mo_9O_{34}]\cdot 2H_2O$				
$[Cu(dap)_2]_4[Cu(dap)_2(H_2O)][Cu(dap)_2(As^{III}As^{V}Mo_9O_{34})_2]\cdot 2H_2O$				
$(H_3NCH_2CH_2NH_3)_2(H_3O)_2[As^{III}As^{V}Mo^{VI}{}_9O_{34}]$ [36]	130	Hydrothermal conditions	$As_2O_3 : Na_2MoO_4\cdot 2H_2O$: ethylenediamine =1 : 1 : 1.5	4.4
$[C_5H_6N]_6[HAs^{III}As^{V}Mo^{V}Mo^{VI}{}_8O_{34}]\cdot 3H_2O$ [37]	130	Hydrothermal conditions	$NaAsO_2 : Na_2MoO_4\cdot 2H_2O$: pyridine = 2 : 1 : 2	5.0
$Co^{III}(en)3H_3O[(Co^{II}O_6)Mo^{VI}{}_6O_{18}(As^{III}{}_3O_3)_2]\cdot 2H_2O$ [21]	135	Hydrothermal conditions	$As_2O_3 : MoO_3\cdot H_2O$: ethylenediamine =1.2 : 1 : 1.2	5.4
$[Cu(imi)_2]_2[(CuO_6)(As_3O_3)_2Mo_6O_{18}][Cu(imi)_2]_2$ [38]	140	Hydrothermal conditions	$NaAsO_2 : (NH_4)_6Mo_7O_{24}\cdot 2H_2O$: imidazole=3.1 : 1.0 : 4.0	–
$[H_4As^{III}{}_2As^{V}Mo^{V}{}_8Mo^{VI}{}_4O_{40}]^{-}$ [20]	150	Hydrothermal conditions	$As_2O_3 : MoO_3 : NaCl$: H_2O = 5 : 10 : 10 : 380	–
$[\{Cu(imi)_2\}_3As_3Mo_3O_{15}]\cdot H_2O$ [23]	160	Hydrothermal Conditions	$NaAsO_2 : (NH_4)_6Mo_7O_{24}\cdot 2H_2O$: imidazole = 3.1 : 0.6 : 4.0	–
$[As(phen)]_2[As_2Mo_2O_{14}]$ [39]	180	Hydrothermal conditions	$NaAsO_2 : H_2MoO_4$: 1,10-phenanthroline = 1.6 : 1.2 : 1	–
(4,4′-bipy)$[Zn(4,4'\text{-bipy})_2(H_2O)_2]_2[(ZnO_6)(As^{III}{}_3O)Mo_6O_{18}]\cdot 7H_2O$(1) [24]	(1)-(4) : 140	Hydrothermal conditions	$NaAsO_2 : Na_2MoO_4\cdot 2H_2O$: 4,4′-bipyridine/2,2′-bipyridine/1,10-phenanthroline = 1 : 1 : 0.5	6.84 6.54
$[Zn(phen)_2(H_2O)]_2[(ZnO_6)(As^{III}{}_3O_3)_2Mo_6O_{18}]\cdot 4H_2O$(2)	(5)-(8) : 130			
$[Zn(2,2'\text{-bipy})2(H_2O)]_2[(ZnO_6)(As^{III}{}_3O_3)_2Mo_6O_{18}]\cdot 4H_2O$(3)				6.68 5.20
$[Zn(H4,4'\text{-bipy})_2(H_2O)_4]\ [(ZnO_6)(As^{III}{}_3O_3)_2Mo_6O_{18}]\cdot 8H_2O$(4)				5.40
$(H_2$4,4′-bipy$)[Cu^{I}(4,4'\text{-bipy})]_2[H_2As^{V}{}_2Mo_6O_{26}]\cdot H_2O$(5)				3.25
$(H_2$4,4′-bipy$)_3[H_2As^{V}{}_2Mo_6O_{26}]\cdot 4H_2O$(6)				
$(H_2$4,4′-bipy$)_3[As^{V}{}_2Mo_6O_{26}]\cdot 4H_2O$(7)				
$(H_2$4,4′-bipy$)_{2.5}(H_3O)[As^{V}{}_2Mo_6O_{26}(H_2O)]\cdot 1.25H_2O$ (8)				3.46 3.42
$[AgAs_2Mo_{15}O_{54}]^{11-}$ [26]	90	solvent evaporation	$As_2O_3 : (NH_4)_6Mo_7O_{24}\cdot 2H_2O$: $AgNO_3$ = 1 : 2 : 1	7.0

During the preparation of {As-O-Mo}, we found that temperature controls the As^{III} being partially oxidized in the final products at 130 °C, resulting in coexistence of As^{III} and As^{V} in $[As^{III}As^{V}Mo_9O_{34}]^{6-}$ [27]. When temperature was higher than 150 °C, As^{III} being oxidized entirely led to the formation of two 1-D chain AMs $[Cu(phen)(H_2O)_2]_2[H_2As^{V}{}_2Mo_6O_{26}]$ [31] and $[Cu_4(en)_4O_2(H_2O)_2][H_2As^{V}{}_2Mo_6O_{26}]$ [32]. When the system temperature was lowered to 90 °C, As^{III} remain stable in the AM fragment, and we obtained a di-capped Anderson-type POM $(H_2en)_3[(NiO_6)Mo_6O_{18}(As_3O_3)_2]Cl_2{\cdot}6H_2O$ [33]. The above conclusion can be also supported by previous reports [20–27,33–39], which are listed in table 2, and the representative complexes are shown in figure 1.

1,10-Phenanthroline serves as an inhibitor, preventing As^{III} from being oxidized to some extent [24]. To investigate the effect of pH on final products, a series of parallel experiments have been carried out; **1** was obtained in the pH range of 5.0–6.5, the most optimal pH was 6.0. When the pH value was lower than 5.0 or higher than 6.5, we only obtained amorphous powers.

Reaction temperature, organic ligands and pH contribute to As^{III} being partially oxidized in the final products, especially the temperature. Finally, the monocapped trivacant Keggin $[As^{III}As^{V}Mo_9O_{34}]^{6-}$ fragment was obtained in the formation of **1**.

3.2. *Crystal structures of 1*

Single-crystal X-ray diffraction analysis reveals that the structural unit of **1** (figure 2(a)) consists of a monocapped trivacant fragment [A-α-$As^{III}As^{V}Mo_9O_{34}]^{6-}$ (figure 2(d)) linked by one $[Ni(en)_2]^{2+}$ (figure 2(b)) and one $[Ni(en)_2(H_2O)]^{2+}$ (figure 2(c)) via bridging oxygens. In the structure of **1**, tetrahedral $\{AsO_4\}$ (figure 2(e)) is located in the center of

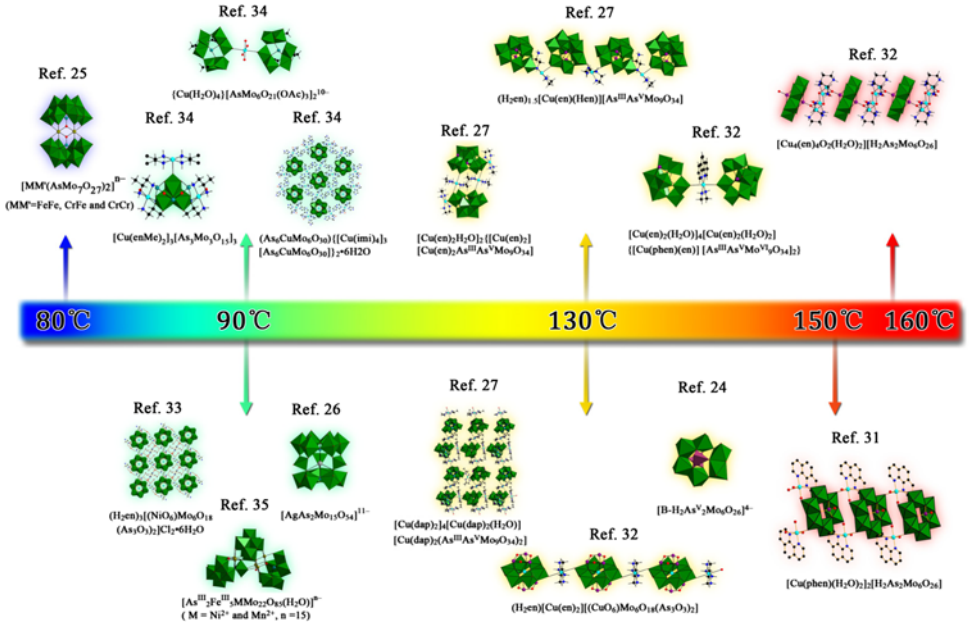

Figure 1. Summary of some representative AM fragments originated from As^{III} relevant to temperature.

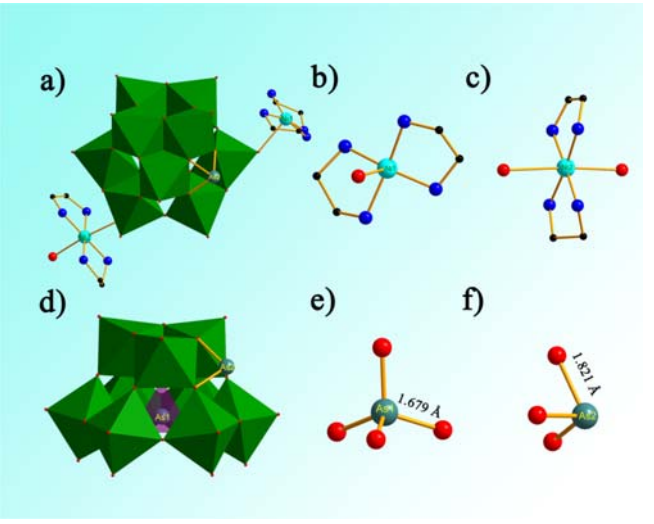

Figure 2. (a) Combined polyhedral/ball-and-stick representation of **1**. (b) The coordination mode of $Ni1^{2+}$. (c) The coordination mode of $Ni2^{2+}$. (d) Combined polyhedral/ball-and-stick representation of [A-α-$As^{III}As^{V}Mo_9O_{34}]^{6-}$ subunit. (e) The tetrahedral $\{AsO_4\}$ group in **1**. (f) The triangular pyramidal $\{AsO_3\}$ group in **1**. Lattice waters are omitted for clarity. Color code: MoO_6 octahedra: green; As: teal; Ni: turquoise; N: blue; O: red; C: black. (see http://dx.doi.org/10.1080/00206814.2013.770484 for color version.)

$[A\text{-}\alpha\text{-}As^{V}Mo_9O_{34}]^{9-}$ and shares four oxygens with three $\{Mo_2O_{10}\}$ groups and a $\{Mo_3O_{13}\}$ triad; the $\{AsO_3\}$ group (figure 2(f)) caps the square window of the $[A\text{-}\alpha\text{-}As^{V}Mo_9O_{34}]^{9-}$ fragment surrounded by a $\{Mo_3O_3\}$ cluster and a $\{Mo_2O_{10}\}$ group. The three oxygens of $\{AsO_3\}$ are in two kinds of chemical environments: one oxygen belonging to bridging oxygen within the $\{Mo_3O_{13}\}$ unit, while the other two oxygens are bridging between $\{Mo_3O_{13}\}$ and $\{Mo_2O_{10}\}$. Therefore, the As–O bond distances in $\{AsO_3\}$ can be classified into two kinds, two short As–O bond distances (As(2)–O(19): 1.799(6) Å and As(2)–O(24): 1.807(6) Å) and one long As–O distance of 1.857(6) Å (As(2)–O(30)), average: 1.821 Å. The triply bridging oxo-group (O(30)) associated with the long As–O bond exhibits pyramidal geometry and those associated with short As–O distances are more nearly trigonal planar. In the central $\{AsO_4\}$ tetrahedron, As(1)–O bond distances are 1.667(6)–1.685(6) Å, average: 1.679 Å. On the basis of valence sum (∑s) calculations [40], the oxidation states of Mo are +6 (∑s = 5.95–6.28), As1 associated with $\{AsO_4\}$ tetrahedron is +5 (∑s = 5.08), As2 associated with the triangular pyramidal $\{AsO_3\}$ group is +3 (∑s = 2.76), and Ni are +2. Ni^{2+} exhibits two kinds of coordination modes, rare in reported POMs (figure 2(b) and (c)).

The striking feature is that **1** contains a monocapped trivacant Keggin $[As^{III}As^{V}Mo_9O_{34}]^{6-}$ (figure 2(d)), which is derived from the rare trivacant Keggin $[A\text{-}\alpha\text{-}As^{V}Mo_9O_{34}]^{9-}$ (figure 3(a)) capped by a triangular pyramidal $\{AsO_3\}$ group. The $[A\text{-}\alpha\text{-}As^{III}As^{V}Mo_9O_{34}]^{6-}$ unit in **1** is different from the monocapped trivacant $[A\text{-}\beta\text{-}As^{III}As^{V}Mo_9O_{34}]^{6-}$ isomer reported in 1999 [36], which is a derivative from the common trivacant Keggin $[A\text{-}\beta\text{-}As^{V}Mo_9O_{34}]^{9-}$ (figure 3(b)). Compared with the $[A\text{-}\beta\text{-}As^{V}Mo_9O_{34}]^{9-}$ fragment, the $[A\text{-}\alpha\text{-}As^{V}Mo_9O_{34}]^{9-}$ can be obtained by the $\{Mo_3O_{13}\}$ trimer of the former rotating 60°. It is obvious that A-α-type or A-β-type trivacant Keggin fragment is derived from removal of a $\{Mo_3O_{13}\}$ trimer from the saturated A-α-Keggin-type or A-β-Keggin-type (figure 3(c) and (d)). It is rare that the A-α-type trivacant Keggin fragment is stable in

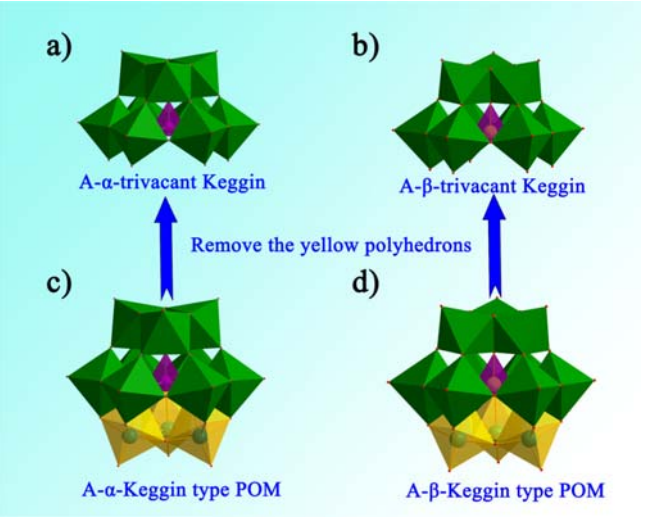

Figure 3. (a) Polyhedral representation of the trivacant Keggin fragment [A-α-$As^{V}Mo_9O_{34}]^{9-}$. (b) Polyhedral representation of the trivacant Keggin fragment [A-β-$As^{V}Mo_9O_{34}]^{9-}$. (c) Polyhedral representation of the $[A\text{-}\alpha\text{-}AsMo_{12}O_{40}]^{3-}$ Keggin type. (d) Polyhedral representation of the $[A\text{-}\beta\text{-}AsMo_{12}O_{40}]^{3-}$ Keggin type. Lattice waters are omitted for clarity. Color code: MoO_6 octahedra: green; As: violet tetrahedron. (see http://dx.doi.org/10.1080/00206814.2013.770484 for color version.)

the solid structure. Only $NaAsO_2$ served as As^{III} starting material, whereas As^{V} was observed in the $[As^{III}As^{V}Mo_9O_{34}]^{6-}$ fragment. Therefore, part of $NaAsO_2$ must be oxidized during the course of the reaction. Similar phenomenon can be observed in previous reports [18,41].

Design of supramolecular architectures is of interest in supramelocular chemistry and crystal engineering because they can provide topology structures and functional materials [42–45]. Keggin-based supramolecular architectures serve as promising materials potentially applied in chemistry, biology and material sciences [46,47]. From the viewpoint of supramolecular chemistry, taking into consideration strong hydrogen-bonding interactions between N of en and O of $[As^{III}As^{V}Mo_9O_{34}]^{6-}$ fragments or water molecules, the 3-D supramolecular structure of **1** is generated through N–H···O hydrogen bonds with N···O distances of 2.687–3.393 Å and N–H···O angles of 123.63°–171.95° (figure 4). Hydrogen-bonding interactions play an important role in stabilization of 3-D supramolecular architecture.

3.3. *XRPD spectrum*

The phase purity of **1** was confirmed by a comparison of the experimental XRPD pattern with the simulated pattern from single-crystal X-ray diffraction (Supplementary material). Owing to variation in preferred orientation of the powder sample during collection of the experimental XRPD, the intensities of the experimental and simulated XRPD patterns are different.

3.4. *IR spectrum*

The IR spectrum of **1** (Supplementary Material) is recorded between 400 and 4000 cm^{-1} with KBr pellet, useful for the identification of characteristic vibration bands of POMs and

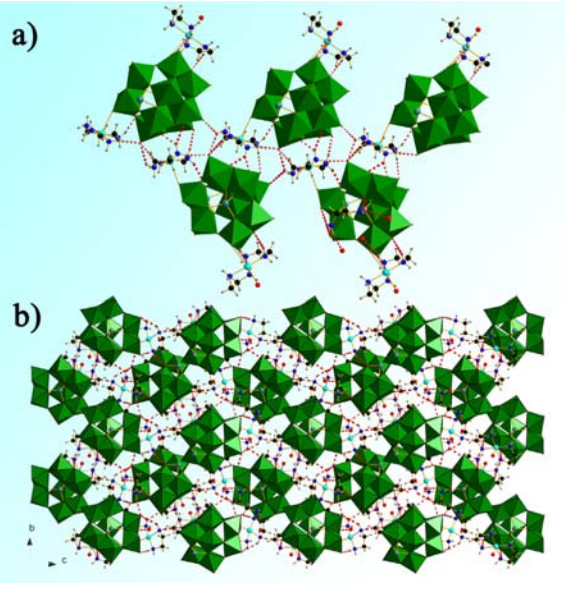

Figure 4. (a) The connection mode of hydrogen bonds between $[Ni(en)_2(H_2O)]\{[Ni(en)_2][As^{III}As^{V}Mo_9O_{34}]^{2+}$ units. (b) Polyhedral and ball-stick representation of the 3-D supramolecular framework structure of **1** via hydrogen bonds.

organic components. Four characteristic bands assigned to $\nu(As^{V}–O)$ or $\nu(Mo–O_t)$, $\nu(As^{III}–O)$, $\nu(Mo–O_b)$ and $\nu(Mo–O_c)$ vibrations appear at 868, 836, 753 and 647 cm^{-1}, respectively [24,26,27]. The absorptions centered at 3245 and 3297 cm^{-1} may be attributed to ν(N–H), which confirms the presence of $–NH_2$ of en. The band at 3446 cm^{-1} is attributed to ν(O–H) of water. The IR spectrum is in agreement with the result of X-ray diffraction structural analysis.

3.5. *XPS spectra*

The bond valence sum (BVS) calculations of **1** indicate that the oxidation states of all Mo and Ni atoms are +6 and +2, and the oxidation states of all As atoms are +3, +5, respectively, which are further confirmed by XPS spectra (figure 5). The XPS spectra of **1** for Mo exhibit two peaks with binding energies of 231.5 and 234.6 eV attributed to Mo^{6+} ($3d_{5/2}$) and Mo^{6+} ($3d_{3/2}$), respectively [18, 26]. The spectra of As show two pair of peaks (39.8 and 44.4 eV ascribed to As^{5+} ($3d_{5/2}$) and As^{5+} ($3d_{3/2}$), 38.8 and 43.5 eV are assigned to As^{3+} ($3d_{5/2}$) and As^{3+} ($3d_{3/2}$) [26, 48–53], indicating that valence states for As in **1** are +5 and +3. The XPS spectra of Ni show two peaks with binding energies of 854.9 and 879.5 eV assigned to Ni^{2+} ($2p_{3/2}$) and Ni^{2+} ($2p_{1/2}$), respectively [18]. These XPS estimations obtained on the valence state values are in reasonable consistence with those calculated from BVS calculations and in agreement with the structure analysis.

3.6. *Scanning electron microscope with energy dispersive X-ray*

EDX-SEM has been used to characterize the composition of the compounds. SEM images of **1** as well as the corresponding spectra recorded for the marked areas are provided in

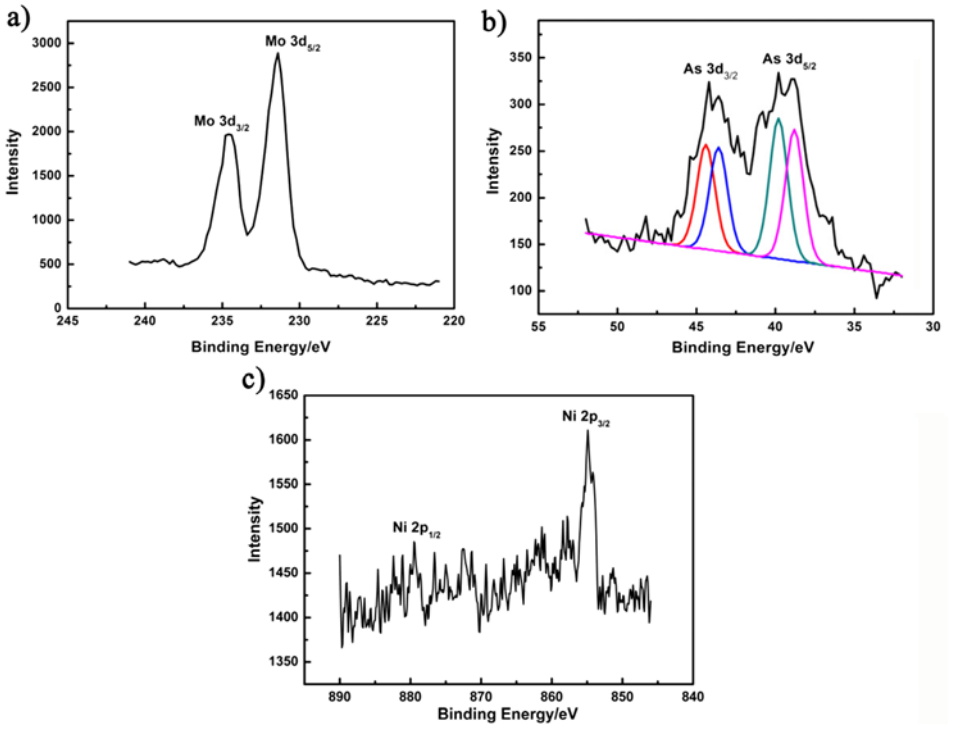

Figure 5. (a) XPS spectra of **1** for Mo $3d_{5/2}$ and Mo $3d_{3/2}$. (b) XPS spectra of **1** for As $3d_{5/2}$ and As$3d_{3/2}$. (c) XPS spectra of **1** for Ni $2p_{3/2}$ and Ni $2p_{1/2}$.

Supplementary Material. According to the EDX spectra, the compositions of the compounds were detected with approximate ratio of Ni : As : Mo of 1.09 : 1.00 : 4.67 for **1**. Owing to error estimated, these results have been checked using multiple samples to reduce the error in the values. We selected four of them in Supplementary Material. Using both the structural data and analysis by EDX, BVS, charge balance arguments, we estimate the formula of **1** is $(H_2en)[Ni(en)_2(H_2O)]\{[Ni(en)_2][As^{III}As^{V}Mo_9O_{34}]\}\cdot 3H_2O$ (Ni : As : Mo = 2 : 2 : 9).

3.7. *Catalytic studies*

Catalytic studies on POMs have received extensive attention [54–56]. We have investigated photodegradation of RhB upon 500 W Xe lamp irradiation for 3 h. In the absence of **1**, RhB aqueous solution hardly degrades (figure 6(a)). On the contrary, when 20 mg of **1** was added to the system in 200 ml (2×10^5 mol L^1) RhB solution, conversion of RhB can reach 97% irradiation for 3 h. The changes in the UV–vis absorption spectra of RhB aqueous solution in the presence of **1** (figure 6(b)) show that the absorbance of RhB ($\lambda = 555$ nm) decreases from 1.23 to 0.02 upon increasing time of irradiation from 0 to 180 min. Correspondingly, figure 6(b) shows that C_t/C_0 decreases with increasing time (C_t is the RhB concentration after given time intervals; C_0 is the RhB concentration at the start of radiation ($t = 0$)). The proposed mechanism may be attributed to: POMs with large band

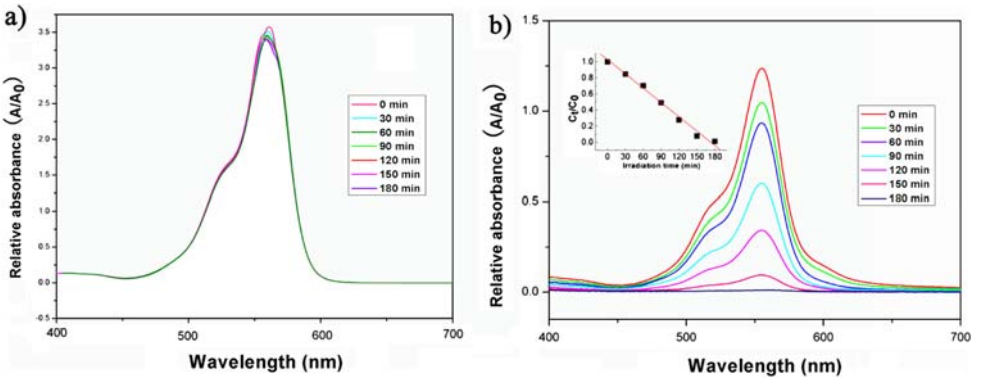

Figure 6. (a) The UVvis absorption spectra of RhB (2×10^5 mol L^1) solution upon 500 W Xe lamp irradiation for 180 min in the absence of **1**. (b) The UVvis absorption spectra of a RhB solution in the presence of **1** as photocatalyst. Inset: Temporal course of the photodegradation of RhB (2×10^5 mol L^1) solution under 500 W Xe lamp irradiation in the presence of **1**.

gaps share photochemical characteristics similar to that of TiO_2 semiconductor producing considerable holes and electrons, which can oxidize the RhB substrate in solution [57, 58]. Reaction of the excited catalyst with H_2O may produce OH radicals that can oxidize the RhB substrate [59,60]. Excitation of the O–M charge transfer band of POMs in the near UV region produces charge transfer from O^2 to Mo^{6+}, forming O and Mo^{5+}. The large surface area of the POM may lead to an increase in catalytic efficiency, for the surface area is an essential factor allowing reactants to be accessible to a great number of active sites.

4. Conclusions

A rare monocapped trivacant fragment $[As^{III}As^{V}Mo_9O_{34}]^{6-}$ has been captured by using TMC under hydrothermal condition, whose successful preparation provides opportunities and guidance in designing and creating novel multi-dimensional hybrid POM materials by modification of traditional fragments. Compound **1** represents the first Ni-substituted inorganic–organic hybrid AM based on $[A\text{-}\alpha\text{-}As^{III}As^{V}Mo_9O_{34}]^{6-}$. The synthesis of **1** not only enrich the diversity of AMs chemistry, but also shows that hydrothermal techniques offer an effective way for making AMs, a promising perspective to develop the family of complexes based on AMs fragment. We will explore further investigation in this domain.

Supplementary material

CCDC 873838 for **1** contains the supplementary crystallographic data for this article. These data can be obtained free of charge from The Cambridge Crystallographic Data Center via www.ccdc.cam.ac.uk/data_request/cif.

Acknowledgements

This study was financially supported by the Natural Science Foundation of China, Special Research Fund for the Doctoral Program of Higher Education, Innovation Scientists and

Technicians Troop Construction Projects of Henan Province, Natural Science Foundation of Henan Province.

References

[1] M.T. Pope. *Inorg. Chem.*, **30**, 181 (1991).
[2] M.T. Pope, A. Müller. *Angew. Chem. Int. Ed.*, **30**, 34 (1991).
[3] M.T. Pope. *Heteropoly and Isopoly Oxometalates*, Springer-Verlag, Berlin (1983).
[4] A. Dolbecq, E. Dumas, C.R. Mayer, P. Mialane. *Chem. Rev.*, **110**, 6009 (2010).
[5] J. Li, Y.F. Qi, J. Li, H.F. Wang, X.Y. Wu, X.Y. Wu, L.Y. Duan, E.B. Wang. *J. Coord. Chem.*, **57**, 1309 (2004).
[6] D.L. Long, R. Tsunashima, L. Cronin. *Angew. Chem. Int. Ed.*, **49**, 1736 (2010).
[7] U. Kortz, N.K. Al-Kassem, M.G. Sacelieff, N.A. Al Kadi, M. Sadakane. *Inorg. Chem.*, **40**, 4742 (2001).
[8] J.L. Xie. *J. Coord. Chem.*, **61**, 3993 (2008).
[9] U. Kortz, M.G. Savelieff, B.S. Bassil, B. Keita, L. Nadjo. *Inorg. Chem.*, **41**, 783 (2002).
[10] L.H. Bi, U. Kortz. *Inorg. Chem.*, **43**, 7961 (2004).
[11] L.L. Chen, L. Zhang, Y.R. Gao, L.Y. Pang, G.L. Xue, F. Fu, J.W. Wang. *J. Coord. Chem.*, **62**, 2832 (2009).
[12] Y.L. Xu, B.B. Zhou, Z.H. Su, K. Yu, J. Wu. *J. Coord. Chem.*, **64**, 3670 (2011).
[13] J.W. Zhao, S.T. Zheng, Z.H. Li, G.Y. Yang. *Dalton Trans.*, **38**, 1300 (2009).
[14] J.X. Meng, Y.G. Li, X.L. Wang, E.B. Wang. *J. Coord. Chem.*, **62**, 2283 (2009).
[15] H.Y. An, T.Q. Xu, X. Liu, C.Y. Jia. *J. Coord. Chem.*, **63**, 3028 (2010).
[16] E. Burkholder, V. Golub, C.J. O'Connor, J. Zubieta. *Inorg. Chem.*, **42**, 6729 (2003).
[17] E. Dumas, C. Debiemme-Chouvy, S.C. Sevov. *J. Am. Chem. Soc.*, **124**, 908 (2002).
[18] S.Z. Li, J.W. Zhao, P.T. Ma, J. Du, J.Y. Niu, J.P. Wang. *Inorg. Chem.*, **48**, 9819 (2009).
[19] Y.Y. Yang, L. Xu, G.G. Gao, F.Y. Li, X.S. Qu, W.H. Guo. *J. Mol. Struct.*, **886**, 85 (2008).
[20] M. Ishaque Khan, Q. Chen, J. Zubieta. *Inorg. Chem.*, **32**, 2924 (1993).
[21] Q.L. He, E.B. Wang. *Inorg. Chim. Acta*, **295**, 244 (1999).
[22] Y.Y. Yang, L. Xu, L.P. Jia, G.G. Gao, F.Y. Li, X.S. Qu, Y.F. Qiu. *Cryst. Res. Technol.*, **42**, 1036 (2007).
[23] Z.F. Zhao, B.-B. Zhou, Z.H. Su, H.Y. Ma, C.X. Li. *Inorg. Chem. Commun.*, **11**, 648 (2008).
[24] C.Y. Sun, Y.G. Li, E.B. Wang, D.R. Xiao, H.Y. An, L. Xu. *Inorg. Chem.*, **46**, 1563 (2007).
[25] H.S. Xu, L.L. Li, B. Liu, G.L. Xue, H.M. Hu, F. Fu, J.W. Wang. *Inorg. Chem.*, **48**, 10275 (2009).
[26] Y.P. Zhang, L.L. Li, T. Sun, B. Liu, H.M. Hu, G.L. Xue. *Inorg. Chem.*, **50**, 2613 (2011).
[27] Q.X. Han, P.T. Ma, J.W. Zhao, Z.L. Wang, W.H. Yang, P.H. Guo, J.P. Wang, J.Y. Niu. *Cryst.Growth Des.*, **11**, 436 (2010).
[28] *SAINT*, Bruker AXS Inc., Madison, WI (2007).
[29] G.M. Sheldrick. *Acta Crystallogr., Sect. A*, **64**, 112 (2007).
[30] G.M. Sheldrick. *SHEXTL-97, Programs for Crystal Structure Refinements*, University of Göttingen, Göttingen (1997).
[31] E. Burkholder, S. Wright, V. Golub, C.J. O'Connor, J. Zubieta. *Inorg. Chem.*, **42**, 7460 (2003).
[32] J.Y. Niu, J.A. Hua, X. Ma, J.P. Wang. *CrystEngComm*, **14**, 4060 (2012).
[33] X. Ma, P.T. Ma, C. Zhang, J.Y. Niu, J.P. Wang. *Chinese Sci. Bull. (Chinese Ver.)*, **56**, 928 (2011).
[34] L.L. Li, B. Liu, G.-L. Xue, H.M. Hu, F. Fu, J.-W. Wang. *Cryst.Growth Des.*, **9**, 5206 (2009).
[35] B. Liu, L.-L. Li, Y.-P. Zhang, Y. Ma, H.M. Huand, G.-L. Xue. *Inorg. Chem.*, **50**, 9172 (2011).
[36] Q. He, E. Wang, W. You, C. Hu. *J. Mol. Struct.*, **508**, 217 (1999).
[37] E.G. Fidalgo, A. Neels, H. Stoeckli-Evans, G. Süss-Fink. *Polyhedron*, **21**, 1921 (2002).
[38] F.Y. Su, B.B. Zhou, Z.F. Zhao, Z.H. Su, C.-C. Zhu. *Cryst. Res. Technol.*, **44**, 447 (2009).
[39] Y.N. Zhang, B.B. Zhou, Z.H. Su, Z.F. Zhao, C.X. Li. *Inorg. Chem. Commun.*, **12**, 65 (2009).
[40] I.D. Brown, D. Altermatt. *Acta Crystallogr., Sect. B*, **41**, 244 (1985).
[41] E.G. Fidalgo, A. Neels, H. Stoeckli-Evans, G. Süss-Fink. *Polyhedron*, **21**, 1921 (2002).
[42] O.M. Yaghi, M. O'Keeffe, N.W. Ockwig, H.K. Chae, M. Eddaoudi, J. Kim. *Nature*, **423**, 705 (2003).
[43] B. Moulton, M.J. Zaworotko. *Chem. Rev.*, **101**, 1629 (2001).
[44] J.Y. Niu, X. Ma, J.W. Zhao, P.T. Ma, C. Zhang, J.P. Wang. *CrystEngComm*, **13**, 4834 (2011).
[45] P.Q. Zheng, Y.P. Ren, L S. Long, R.B. Huang, L.S. Zheng. *Inorg. Chem.*, **44**, 1190 (2005).
[46] Y. Ding, J.X. Meng, W.L. Chen, E.B. Wang. *CrystEngComm*, **13**, 2687 (2011).
[47] J.X. Meng, Y. Lu, Y.G. Li, H. Fu, E.B. Wang. *CrystEngComm*, **13**, 2479 (2011).
[48] L.H. Bi, J.Y. Liu, Y. Shen, J.G. Jiang, S.-J. Dong. *New J. Chem.*, **27**, 75 (2003).
[49] Y. Hou, Y.-G. Wei, D.G. Xiao, E.H. Shen, E.B. Wang, Y.G. Li, L. Xu, C.W. Hu. *Inorg. Chim. Acta*, **357**, 2477 (2004).
[50] Y. Hou, Y.G. Wei, E.H. Shen, D.G. Xiao, E.B. Wang, S.T. Wang, Y.G. Li, L. Xu, C.-W. Hu. *Inorg. Chem. Commun.*, **4**, 128 (2004).

[51] Y. Hou, S.T. Wang, E.H. Shen, D.G. Xiao, E.B. Wang, Y.G. Li, L. Xu, C.W. Hu. *J. Mol. Struct.*, **689**, 81 (2004).
[52] S.Y. Shi, Y. Chen, J.N. Xu, Y.C. Zou, X.B. Cui, Y. Wang, T.G. Wang, J.Q. Xu, Z.-M. Gao. *CrystEngComm*, **12**, 1949 (2010).
[53] J.P. Wang, P.T. Ma, J.W. Zhao, J.Y. Niu. *Inorg. Chem. Commun.*, **10**, 523 (2007).
[54] I. Texier, J. Ouazzani, J. Delaire, C. Giannotti. *Tetrahedron*, **55**, 3401 (1999).
[55] I. Texier, C. Giannotti, S. Malato, C. Richter, J. Delaire. *Catal. Today*, **54**, 297 (1999).
[56] C.C. Chen, W. Zhao, P.X. Lei, J.C. Zhao, N. Serpone. *Chem.–A Eur. J.*, **10**, 1956 (2004).
[57] A. Hiskia, A. Mylonas, E. Papaconstantinou. *Chem. Soc. Rev.*, **30**, 62 (2010).
[58] Y.L.J. You, S.Y. Gao, B. Xu, G.L. Li, R. Cao. *J. Colloid Interf. Sci.*, **2**, 562 (2010).
[59] J.A. Schwarz. *Chem. Rev.*, **95**, 477 (1995).
[60] N. Mizuno, M. Misono. *Chem. Rev.*, **98**, 99 (1998).